

PET monitoring of cancer therapy with ^3He and ^{12}C beams: a study with the GEANT4 toolkit

Igor Pshenichnov^{1,2}, Alexei Larionov^{1,3}, Igor Mishustin^{1,3}
and Walter Greiner¹

¹ Frankfurt Institute for Advanced Studies, Johann Wolfgang Goethe University,
60438 Frankfurt am Main, Germany

² Institute for Nuclear Research, Russian Academy of Science, 117312 Moscow,
Russia

³ Kurchatov Institute, Russian Research Center, 123182 Moscow, Russia

Abstract. We study the spatial distributions of β^+ -activity produced by therapeutic beams of ^3He and ^{12}C ions in various tissue-like materials. The calculations were performed within a Monte Carlo model for Heavy-Ion Therapy (MCHIT) based on the GEANT4 toolkit. The contributions from positron-emitting nuclei with $T_{1/2} > 10$ s, namely $^{10,11}\text{C}$, ^{13}N , $^{14,15}\text{O}$, $^{17,18}\text{F}$ and ^{30}P , were calculated and compared with experimental data obtained during and after irradiation, where available. Positron emitting nuclei are created by ^{12}C beam in fragmentation reactions of projectile and target nuclei. This leads to a β^+ -activity profile characterised by a noticeable peak located close to the Bragg peak in the corresponding depth-dose distribution. This can be used for dose monitoring in carbon-ion therapy of cancer. On the contrary, as the most of positron-emitting nuclei are produced by ^3He beam in target fragmentation reactions, the calculated total β^+ -activity during or soon after the irradiation period is evenly distributed within the projectile range. However, we predict also the presence of ^{13}N , ^{14}O , $^{17,18}\text{F}$ created in charge-transfer reactions by low-energy ^3He ions close to the end of their range in several tissue-like media. The time evolution of β^+ -activity profiles was investigated for both kinds of beams. We found that due to the production of ^{18}F nuclide the β^+ -activity profile measured 2 or 3 hours after irradiation with ^3He ions will have a distinct peak correlated with the maximum of depth-dose distribution. We also found certain advantages of low-energy ^3He beams over low-energy proton beams for reliable PET monitoring during particle therapy of shallow located tumours. In this case the distal edge of β^+ -activity distribution from ^{17}F nuclei clearly marks the range of ^3He in tissues.

Submitted to: *Phys. Med. Biol.*

PACS numbers: 87.53.Pb, 87.53.Wz, 87.53.Vb

E-mail: pshenich@fias.uni-frankfurt.de

1. Introduction

Beams of protons and carbon ions are used in particle therapy of deep-seated tumours for conformal irradiation of a tumour volume while sparing surrounding healthy tissues and organs at risk (Castro *et al* 2004, Amaldi and Kraft 2005). New facilities for proton and ion therapy of cancer are planned or under construction in France (Bajard

et al 2004), in Italy (Amaldi 2004), in Austria (Griesmayer and Auberger 2004) and in Germany (Haberer *et al* 2004). Along with other facilities the Heidelberg Ion Therapy Center (HIT) (Haberer *et al* 2004, Heeg *et al* 2004) will use several beams for treatment: protons, ^3He , carbon and oxygen nuclei. There oncologists will have a variety of treatment tools at their disposal, while each treatment option will be characterised by its specific effectiveness, possible side effects and treatment costs. Appropriate quality assurance methods should be also developed specifically for each kind of treatment.

In particular, the Positron Emission Tomography (PET) during or after irradiation provides the possibility to monitor the delivered dose. The PET monitoring methods in proton and ion therapy can be divided into two categories: (i) based on tracing the positron emitting nuclei, e.g. ^{10}C , ^{11}C and ^{15}O , created by proton beams in tissues due to fragmentation of *target nuclei*; (ii) based on tracing the positron emitting nuclei, ^{10}C and ^{11}C , created in fragmentation reactions of ^{12}C *beam nuclei*. The spatial distribution of positron emitting nuclei is measured by detecting gamma pairs from $e^+e^- \rightarrow \gamma\gamma$ annihilation events. By comparing the measured β^+ -activity distribution with the distribution calculated for the planned dose, one can control the accuracy of the actual treatment.

Following extensive theoretical and experimental studies with carbon beams (Enghardt *et al* 1992, Pawelke *et al* 1996, Pawelke *et al* 1997, Pönisch *et al* 2004, Parodi 2004), in-beam PET monitoring is successfully used in carbon-ion therapy at GSI, Darmstadt, Germany (Enghardt *et al* 2004, Schulz-Ertner *et al* 2004). Similar approaches can be used for monitoring of proton therapy, as shown early by Bennett *et al* 1975, Bennett *et al* 1978 and later by Oelfke *et al* 1996, Parodi and Enghardt 2000, Parodi *et al* 2002, Parodi 2004, Nishio *et al* 2005, Parodi *et al* 2007a and Parodi *et al* 2007b. PET images from proton and carbon-ion therapy were also studied in experiments by Hishikawa *et al* 2004 at Hyogo ion therapy centre in Japan (Hishikawa *et al* 2002).

Beams of nuclei lighter than carbon, e.g. ^3He , ^4He or ^7Li , are also of clinical interest. This is shown, in particular, by Furusawa *et al* 2000 and Kempe *et al* 2007. An advantage of ^3He nuclei consists in their specific $Z/A = 2/3$ ratio which helps to protect the ^3He beam from contamination with ^4He , ^{12}C , ^{16}O nuclei. The feasibility of in-beam PET for ^3He therapy was demonstrated for the first time in experiments by Fiedler *et al* 2006.

In the present work we use a Monte Carlo model for Heavy-Ion Therapy (MCHIT) (Pshenichnov *et al* 2005, 2006) based on the GEANT4 simulation toolkit (Agostinelli *et al* 2003, Allison *et al* 2006) to study the β^+ -activity profiles induced by ^3He and ^{12}C beams in tissue-like media. We argue that specific nuclear reactions, namely *proton pick-up by target nuclei*, play certain role in production of positron emitting nuclei by ^3He beams in addition to previously studied nuclear fragmentation reactions. In Section 2 we describe the physical models from the GEANT4 toolkit used to build MCHIT. In Section 3 the time-dependent analysis of the β^+ -activity distributions induced by ^3He and ^{12}C beams in graphite, water and PMMA phantoms is presented. In Section 4 calculational results are compared with experimental data obtained by Fiedler *et al* 2006. Results for homogeneous phantoms with stoichiometric composition of muscle and bone tissues are presented in Section 5. The calculated distributions of β^+ -activity induced by low energy proton, ^3He and ^{12}C beams are discussed in Section 6 with emphasis on the role of proton pick-up reactions induced by ^3He . In Section 7 the reliability of MCHIT results is verified by comparison with available

experimental data on specific reaction cross sections and isotope yields in thick targets. Section 8 contains summary and conclusions.

2. GEANT4 physics models used in MCHIT

We have used the version 8.2 of the GEANT4 toolkit (GEANT4-Webpage 2006) to build a Monte Carlo model for Heavy-Ion Therapy (MCHIT). The model is intended for calculating the spatial distributions of dose and β^+ -activity from beams of light nuclei (from protons to oxygen ions) in homogeneous tissue-like media. The phantom material and size, as well as beam parameters such as energy spread, transverse beam size, emittance, angular divergence, can be set via user interface commands.

In MCHIT the energy loss and straggling of primary and secondary charged particles due to interaction with atomic electrons is described via a set of models called 'standard electromagnetic physics'. Multiple scattering due to electromagnetic interactions with atomic nuclei is also included in simulations.

In each simulation step, the ionisation energy loss of a charged particle is calculated according to the Bethe-Bloch formula. The average excitation energy of the water molecule was set to 77 eV, i.e. to the value which better describes the set of available data on depth-dose distributions for therapeutic proton and carbon-ion beams. This parameter was taken 68.5 eV for PMMA, 78 eV for graphite, 86.5 eV for bone tissue and 70.9 eV for muscle tissue.

Two kinds of hadronic interactions are considered in the MCHIT model: (a) elastic scattering of hadrons on target protons and nuclei, which dominate at low projectile energies, and (b) inelastic nuclear reactions induced by fast hadrons and nuclei (GEANT4-Documents 2006).

The overall probability of hadronic interactions for nucleons and nuclei propagating through the medium depends on the total inelastic cross section for proton-nucleus and nucleus-nucleus collisions. Parametrised equations by Wellisch and Axen 1996 that best fit experimental data were used to describe the total reaction cross sections in nucleon-nucleus collisions. Systematics by Tripathi *et al* 1997 and Shen *et al* 1989 for the total nucleus-nucleus cross sections were used for calculating the probability of nucleus-nucleus collisions.

In the MCHIT model the inelastic interaction of nucleons below 20 MeV is simulated by means of data driven models. Above 20 MeV the exciton-based precompound model is invoked (Agostinelli *et al* 2003, Allison *et al* 2006). For hadrons and nuclei with the energies above 80 MeV, we employed the binary cascade model (Folger *et al* 2004). Excited nuclear remnants are created after the first cascade stage of interaction. Therefore, appropriate models for describing the de-excitation process have to be involved into simulation. The Weisskopf-Ewing model (Weisskopf and Ewing 1940) was used to describe the evaporation of nucleons from residual nuclei at relatively low excitation energies, below 3 MeV per nucleon. The Statistical Multifragmentation Model (SMM) by Bondorf *et al* 1995 was used at excitation energies above 3 MeV per nucleon to describe the multi-fragment break-up of highly-excited residual nuclei. The SMM includes as its part the Fermi break-up model, which describes the explosive decay of highly-excited light nuclei.

3. Time-dependent analysis of the β^+ activity

We follow the approach of Parodi *et al* 2002 in calculating the time dependence of β^+ -activity induced by therapeutic beams. As reported by Fiedler *et al* 2006, the time structure of ion beams provided by the GSI synchrotron consists of repeated particle extractions (spills) and pauses. It is assumed in calculations, that each beam spill has duration of τ_s with the average intensity of J (ions/s) during the beam extraction. The irradiation procedure consists of N spills with pauses between subsequent spills of τ_p , as given in Table 1. Both τ_s and τ_p are in the range of 1-3 s.

Table 1. Beam parameters for 207.92 A MeV ^3He and 337.5 A MeV ^{12}C used for irradiation of graphite, water and PMMA phantoms by Fiedler *et al* 2006. It is denoted: N — number of spills, J — beam intensity during each spill, τ_s — spill duration, τ_p — duration of a pause between spills.

Projectile	Phantom material	N	J (10^8 s^{-1})	τ_s (s)	τ_p (s)
^3He	graphite	120	1.9	1.39	3.10
^3He	water	99	2.0	1.35	3.14
^3He	PMMA	120	2.0	1.37	3.12
^{12}C	graphite	120	0.9	2.20	2.29
^{12}C	water	120	0.9	2.20	2.29
^{12}C	PMMA	120	0.9	2.19	2.30

The depth distributions $dn_i(z)/dz \equiv f_i(z)$ of positron-emitting isotopes of species i along the beam axis z produced per beam particle were calculated with the MCHIT model. These distributions refer to the secondary nuclei at their stopping points in the medium. Then, the depth distribution of the i -th isotope $dN_i(z, t)/dz \equiv F_i(z, t)$ during the irradiation is expressed as a function of time:

$$\frac{\partial F_i(z, t)}{\partial t} = Jf_i(z) - \lambda_i F_i(z, t) \quad \text{for } t_j - \tau_s \leq t < t_j, \quad (1)$$

$$\frac{\partial F_i(z, t)}{\partial t} = -\lambda_i F_i(z, t) \quad \text{for } t_j \leq t < t_j + \tau_p, \quad (2)$$

where λ_i is the decay constant of the i -th isotope, $\lambda_i = \ln(2)/T_{1/2}^i$, where $T_{1/2}^i$ is the half-life of the i -th isotope, and $t_j \equiv \tau_s + (\tau_p + \tau_s)(j - 1)$ is the time when the j -th spill ends, $j = 1, \dots, N$. Eqs.(1) and (2) describe the production and decay of the i -th isotope during the j -th spill and j -th pause, respectively. After the irradiation i -th isotope decays exponentially:

$$F_i(z, t) = F_i(z, t_N) \exp(-\lambda_i(t - t_N)) \quad \text{for } t \geq t_N. \quad (3)$$

The system (1),(2) can be solved recursively (c.f. Parodi *et al* 2002):

$$F_i(z, t_j) = F_i(z, t_{j-1}) \exp(-\lambda_i(\tau_p + \tau_s)) + F_i(z, t_1) \quad \text{for } j = 2, \dots, N, \quad (4)$$

$$F_i(z, t_1) = \frac{Jf_i(z)}{\lambda_i} (1 - \exp(-\lambda_i\tau_s)). \quad (5)$$

This gives the following expression for the depth distribution of the i -th isotope at the end of j -th spill:

$$F_i(z, t_j) = F_i(z, t_1) \sum_{n=0}^{j-1} \exp(-\lambda_i(\tau_p + \tau_s)n) \quad \text{for } j = 1, \dots, N. \quad (6)$$

Since the measurements of the β^+ -activity during the irradiation were performed only in pauses between subsequent spills, the total number of β^+ -decays per unit depth during the irradiation is

$$\frac{dN_{\beta^+}}{dz} = \sum_i (1 - \exp(-\lambda_i \tau_p)) \sum_{j=1}^{N-1} F_i(z, t_j) . \quad (7)$$

After the irradiation the measurements were performed in the time interval from t_{st} to t_{fin} continuously, thus

$$\frac{dN_{\beta^+}}{dz} = \sum_i F_i(z, t_N) [\exp(-\lambda_i(t_{st} - t_N)) - \exp(-\lambda_i(t_{fin} - t_N))] . \quad (8)$$

The half-life times of the isotopes included in our analysis and listed in the next section are much longer than the spill duration and the pause between spills: $(\tau_s + \tau_p)\lambda_i \ll 1$. Under this condition Eqs. (7) and (8) can be simplified. The number of β^+ -decays per unit length during the irradiation becomes

$$\frac{dN_{\beta^+}}{dz} \simeq \sum_i \bar{J} f_i(z) \frac{\tau_p}{\tau_p + \tau_s} \left[t_N - \frac{1}{\lambda_i} (1 - \exp(-\lambda_i t_N)) \right] , \quad (9)$$

while after the irradiation

$$\begin{aligned} \frac{dN_{\beta^+}}{dz} \simeq \sum_i \frac{\bar{J} f_i(z)}{\lambda_i} (1 - \exp(-\lambda_i t_N)) \\ \times [\exp(-\lambda_i(t_{st} - t_N)) - \exp(-\lambda_i(t_{fin} - t_N))] . \end{aligned} \quad (10)$$

Here $\bar{J} \equiv J\tau_s/(\tau_p + \tau_s)$ is the average beam intensity calculated for the whole irradiation period.

4. Comparison of numerical results with experimental data

4.1. Depth distributions of β^+ -activity

The spatial distributions of the β^+ -activity induced by 207.92 A MeV ^3He and 337.5 A MeV ^{12}C in various phantoms were measured by Fiedler *et al* 2006. In order to validate the MCHIT model with these data we performed calculations for graphite ($9 \times 9 \times 15 \text{ cm}^3$, $\rho = 1.795 \text{ g cm}^{-3}$), water with an admixture of gelatine ($\text{H}_{66.2}\text{O}_{33.1}\text{C}_{0.7}$, $9 \times 9 \times 30 \text{ cm}^3$, $\rho = 1.0 \text{ g cm}^{-3}$) and polymethyl methacrylate (PMMA, $\text{C}_5\text{H}_8\text{O}_2$, $9 \times 9 \times 20 \text{ cm}^3$, $\rho = 1.18 \text{ g cm}^{-3}$) phantoms.

Monte Carlo calculations with the MCHIT model have provided the depth distributions in the phantoms for the following positron-emitting nuclei with $T_{1/2} > 10 \text{ s}$: ^{10}C ($T_{1/2} = 19.255 \text{ s}$), ^{11}C ($T_{1/2} = 20.39 \text{ min}$), ^{13}N ($T_{1/2} = 9.965 \text{ min}$), ^{14}O ($T_{1/2} = 1.177 \text{ min}$), ^{15}O ($T_{1/2} = 2.04 \text{ min}$), ^{17}F ($T_{1/2} = 1.075 \text{ min}$), ^{18}F ($T_{1/2} = 109.77 \text{ min}$). It was found that these are the most abundant positron-emitting nuclei produced by ^3He and ^{12}C in graphite, water and PMMA. Much lower yields were found for ^8B , ^9C , ^{12}N and ^{13}O . Moreover, as the latter isotopes have rather short half-life time $T_{1/2} < 1 \text{ s}$, they decay during the beam spills and do not produce any significant contribution during pauses when Fiedler *et al* 2006 performed their measurements.

The calculated depth distribution of β^+ -activity for 207.92 A MeV ^3He beam in graphite, water and PMMA are shown in Figs. 1, 2 and 3 and compared to the data obtained by Fiedler *et al* 2006 during irradiation and from 10 to 20 min after it. Since measured distributions were presented in arbitrary units, in Figs. 1, 2 and 3 they

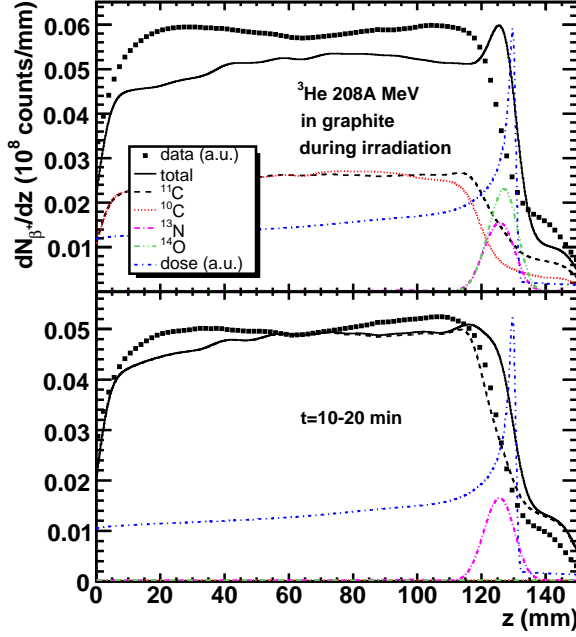


Figure 1. Depth distribution of β^+ -activity induced by 207.92 A MeV ^3He beam in graphite. The distributions of β^+ -decays counted during irradiation and from 10 to 20 min after it are shown by solid lines in top and bottom panels, respectively. Data by Fiedler *et al* 2006 are shown by points. Contributions of specific isotopes and depth-dose distribution are also shown, as explained on the legend.

were normalised to the corresponding maxima of the calculated dN_{β^+}/dz distributions during irradiation. The same weight factor was applied for plotting the experimental data after irradiation.

The dN_{β^+}/dz distributions during and after irradiation were calculated according to Eqs.(7) and (8), respectively. The beam parameters quoted in Table 1 were used in calculations. The calculated dN_{β^+}/dz distributions were folded with the Gaussian weight of FWHM=8 mm. This width represents the sum of (1) the average distance between a nucleus which emits a positron and annihilation point ~ 2 mm, (c.f. Levin and Hoffman 1999), and (2) a finite spatial resolution (6.5 ± 2 mm) of the PET scanner used by Fiedler *et al* 2006. The shapes of the β^+ -activity distributions shown in Figs. 1 2 and 3 should be compared with the corresponding depth-dose distributions (given in arbitrary units) in order to investigate the correlation between them.

Figures 1, 2 and 3 demonstrate also the dependence of the β^+ -activity distributions on the elemental composition of the specified target materials. In graphite, which contains only carbon nuclei, mostly ^{11}C and ^{10}C isotopes are produced by ^3He via the removal of one or two neutrons from target ^{12}C nuclei. As shown in Fig. 1, these nuclei are evenly distributed within the range of ^3He projectiles and ^{11}C is the most abundant β^+ -emitter. The MCHIT model predicts a bump near the Bragg peak due to ^{14}O and ^{13}N , which is, however, not visible in the data. A smaller bump

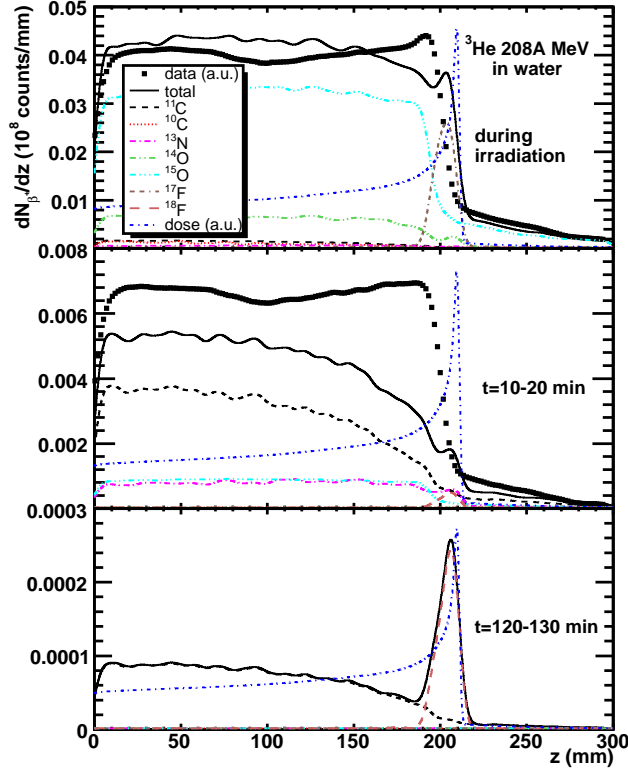


Figure 2. Depth distribution of β^+ -activity induced by 207.92 A MeV ^3He beam in water. The distributions of β^+ -decays counted during irradiation, from 10 to 20 min and from 120 to 130 min after it are shown by solid lines in top, middle and bottom panels, respectively. Data by Fiedler *et al* 2006 are shown by points. Contributions of specific isotopes and depth-dose distribution are also shown, as explained on the legend.

due to ^{13}N is also present in the total β^+ -activity distribution calculated 10-20 min after irradiation.

A larger set of isotopes is produced by ^3He in water, see Fig. 2. The most abundant positron-emitting nuclei are ^{15}O and ^{11}C . While ^{15}O is produced by the removal of a single neutron from a target ^{16}O nucleus, the production mechanism of ^{11}C , via the $^{16}\text{O}(^3\text{He}, 4p4n)^{11}\text{C}$ reaction, is more complicated. This is reflected in the fact that the overall shape of the total β^+ -activity distribution during irradiation is satisfactory reproduced by the MCHIT model since it is mostly due to ^{15}O . However, there is a big discrepancy between theory and experiment for the time interval 10-20 min after irradiation, as shown in the middle panel of Fig. 2. It can be explained by the deficiency of the model in calculating $^{16}\text{O}(^3\text{He}, 4p4n)^{11}\text{C}$ reaction which can proceed through various intermediate states and reaction channels.

The MCHIT model predicts a noticeable contribution to the β^+ -activity from ^{14}O during irradiation of water by ^3He . As the half-life time of ^{14}O is much shorter than that of ^{11}C , ^{14}O gives larger contribution during irradiation, while ^{11}C contribution dominates 10-20 min after irradiation. The model also predicts a small bump close to the Bragg peak due to ^{17}F . A similar but somewhat shifted bump is also seen in the

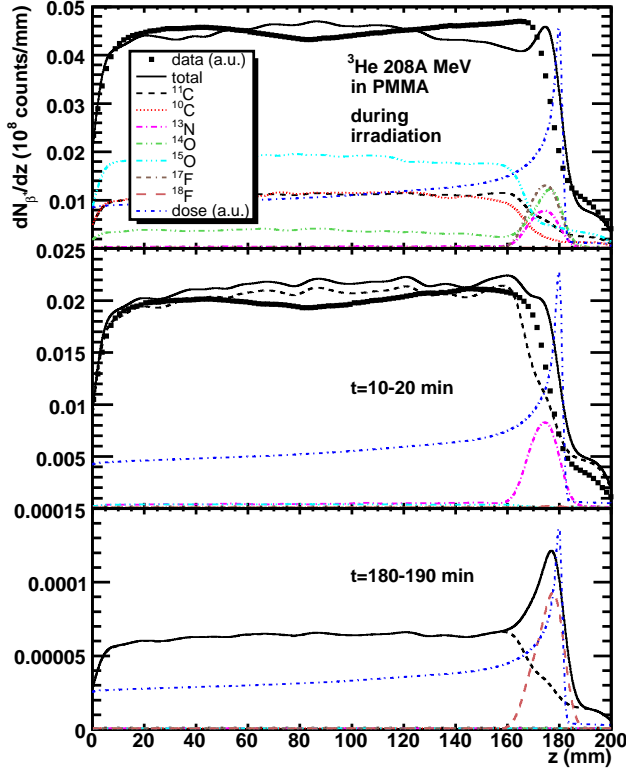


Figure 3. Same as Fig. 2, but for 207.92 A MeV ^3He beam in PMMA and for β^+ -decays counted from 180 to 190 min after irradiation (bottom panel).

data for the total β^+ -activity distribution. The distal slope of the activity distribution can be used for determination of the ^3He range in tissues, similar to the proposal by Parodi *et al* 2002 for therapeutic proton beams.

We have found that a better way to monitor the ^3He range in tissues can be provided by measuring the β^+ -activity at later times, e.g. in the time window of 120-130 min after irradiation. The activity distributions for this time interval are also shown in Fig. 2. Here, the long-living ^{18}F isotope from the $^{16}\text{O}(^3\text{He},p)^{18}\text{F}$ reaction dominates, and the peak in the activity distribution clearly marks the position of the Bragg peak.

As shown in Fig. 3, in PMMA two dominating β^+ -emitters, ^{11}C and ^{15}O , are produced by ^3He . These isotopes are produced in the $^{12}\text{C}(^3\text{He},\alpha)^{11}\text{C}$ and $^{16}\text{O}(^3\text{He},\alpha)^{15}\text{O}$ reactions on carbon and oxygen nuclei from PMMA. Due to PMMA chemical composition, ^{11}C is more abundant than ^{15}O in this material. The activity distribution in PMMA calculated for later times, e.g. 180-190 min after irradiation, also has a bump close to the Bragg peak. This activity peak is due to ^{18}F produced in the $^{16}\text{O}(^3\text{He},p)^{18}\text{F}$ reaction.

The MCHIT model is also verified with the β^+ -activity distributions measured by Fiedler *et al* 2006 for 337.5 A MeV ^{12}C beam in graphite, water and PMMA, as shown in Figs. 4, 5 and 6. In these phantom materials ^{10}C and ^{11}C can be produced by single or double neutron removal from both ^{12}C projectiles and ^{12}C target nuclei. As

a result, the β^+ -activity distribution is characterised by sharp peaks due to projectile fragmentation and plateau due to target fragmentation, as seen, in particular, in Fig. 4.

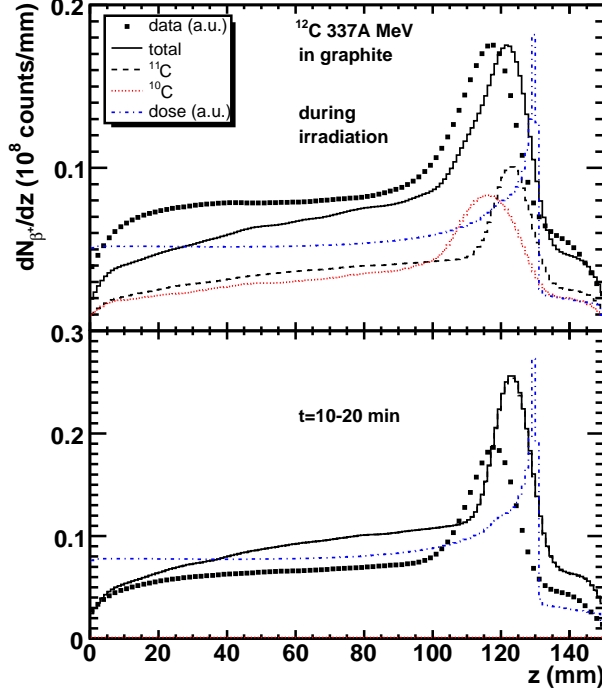


Figure 4. Depth distribution of β^+ -activity induced by 337.5 A MeV ^{12}C beam in graphite. The distributions of β^+ -decays counted during irradiation and from 10 to 20 min after it are shown by solid lines in top and bottom panels, respectively. Data by Fiedler *et al* 2006 are shown by points. Contributions of specific isotopes and depth-dose distribution are also shown, as explained on the legend.

The overall shapes of the total β^+ -activity distributions are satisfactorily described by the MCHIT model. However, as a rule, the peaks in theoretical distributions are located 5-10 mm deeper compared to the experimental ones. This shift is caused by the overestimation of the ^{11}C production in the binary cascade model at low energies, as explained in Section 7.

As seen in Figs. 4, 5 and 6 for all three materials, only ^{11}C survives within 10 min after irradiation. However, during irradiation the contributions from ^{14}O and ^{15}O are important for water and PMMA. These positron-emitting oxygen isotopes are also produced beyond the Bragg peak by energetic secondary protons emitted in nuclear fragmentation of ^{12}C beam.

4.2. Total yields of positron-emitting nuclei produced by ^3He and ^{12}C beams

The MCHIT model can further be validated by confronting calculated total production yields of specific positron-emitting nuclei with the yields measured by Fiedler *et al* 2006. In Tables 2, 3 and 4 we present the total yields of the most abundant isotopes, ^{10}C , ^{11}C , ^{13}N and ^{15}O , produced by ^3He and ^{12}C beams in graphite, water and PMMA phantoms. The values are given in % per beam particle.

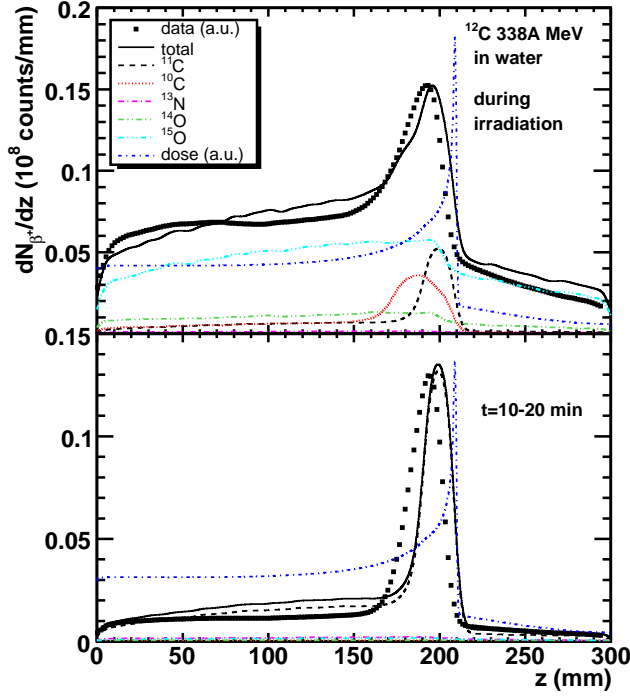


Figure 5. Same as Fig. 4, but for by 337.5 A MeV ^{12}C beam in water.

From inspecting Table 2 one can conclude that the calculated yields of ^{11}C are in better agreement with experiment than ^{10}C yields. The yields of ^{11}C produced by ^3He are well described, while the model overestimates the production of ^{10}C by both beams.

Table 2. Computed number of β^+ -emitters (in % per beam particle) from interactions of ^3He and ^{12}C in graphite. Data are from Fiedler *et al* 2006.

	^3He , 130.03A MeV		^3He , 166.05A MeV		^3He , 207.92A MeV		^{12}C , 337.5A MeV	
	MCHIT	Experiment	MCHIT	Experiment	MCHIT	Experiment	MCHIT	Experiment
^{10}C	0.712	0.44 ± 0.07	1.07	0.69 ± 0.10	1.51	0.98 ± 0.15	4.56	1.88 ± 0.28
^{11}C	5.28	6.9 ± 1.0	7.99	10.0 ± 1.5	11.09	13.9 ± 2.1	34.80	24.9 ± 3.7
^{13}N	0.508	—	0.460	—	0.358	—	0.155	—
^{15}O	0.0021	—	0.0022	—	0.002	—	0.031	—

One can also compare the model with the data on ^{13}N and ^{15}O production in irradiation of water phantoms by ^3He and ^{12}C . Calculated and measured yields for this case are presented in Table 3. The yields of ^{15}O produced by ^3He are underpredicted by the model by $\sim 30\%$ for all ^3He energies, while the production of ^{15}O and ^{11}C by ^{12}C beam is well described. On the other hand, the model completely fails in describing ^{13}N and ^{11}C production by ^3He , as these yields are underestimated by a factor of three. We attribute this problem to the complexity of $^{16}\text{O}(^3\text{He}, 3\text{p}3\text{n})^{13}\text{N}$ and

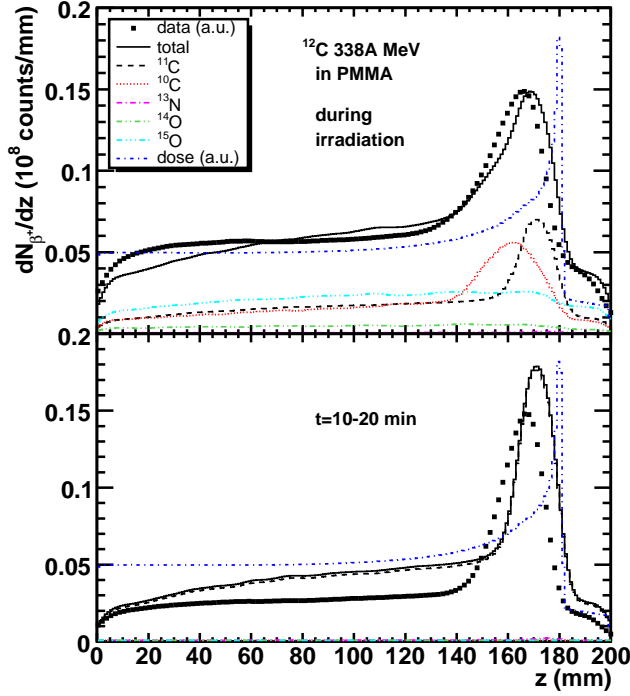


Figure 6. Same as Fig. 4, but for by 337.5 A MeV ^{12}C beam in PMMA.

$^{16}\text{O}(^3\text{He},4\text{p}4\text{n})^{11}\text{C}$ reactions. The ability of the model to predict ^{10}C yields for ^3He beams depends on the beam energy. The calculations agree better with the data at 207.92 A MeV than at 130.03 and 166.05 A MeV.

Table 3. Computed number of β^+ -emitters (in % per beam particle) from interactions of ^3He and ^{12}C in water. Data are from Fiedler *et al* 2006.

	^3He , 130.03A MeV		^3He , 166.05A MeV		^3He , 207.92A MeV		^{12}C , 337.5A MeV	
	MCHIT	Experiment	MCHIT	Experiment	MCHIT	Experiment	MCHIT	Experiment
^{10}C	0.039	0.21 ± 0.03	0.071	0.19 ± 0.03	0.118	0.18 ± 0.04	1.93	0.78 ± 0.12
^{11}C	0.415	1.85 ± 0.28	0.784	2.49 ± 0.37	1.28	3.23 ± 0.48	13.1	12.6 ± 1.9
^{13}N	0.154	0.49 ± 0.07	0.235	0.80 ± 0.12	0.321	1.02 ± 0.15	1.02	2.40 ± 0.36
^{15}O	2.30	4.40 ± 0.66	3.75	6.29 ± 0.94	5.65	8.29 ± 1.24	15.3	14.6 ± 2.2

Calculations and experimental data for PMMA phantoms irradiated by ^3He and ^{12}C are presented in Table 4. The calculated yields of ^{10}C and ^{13}N produced by ^3He in this material are well described by the MCHIT model, while the yields of most abundant ^{11}C and ^{15}O are underestimated by $\sim 30\%$. The model is quite successful in describing ^{13}N , ^{11}C and ^{15}O produced by ^{12}C beam, but the production of ^{10}C is overestimated.

In summary, the yields of the most abundant isotopes ^{11}C and ^{15}O produced by ^{12}C in water and PMMA are very well described by the MCHIT model, see Tables 3 and 4. However, the yields of ^{11}C and ^{15}O , which are abundantly produced also by

Table 4. Computed number of β^+ -emitters (in % per beam particle) from interactions of ^3He and ^{12}C in PMMA. Data are from Fiedler *et al* 2006.

	^3He , 130.03A MeV		^3He , 166.05A MeV		^3He , 207.92A MeV		^{12}C , 337.5A MeV	
	MCHIT	Experiment	MCHIT	Experiment	MCHIT	Experiment	MCHIT	Experiment
^{10}C	0.398	0.38 ± 0.06	0.607	0.53 ± 0.08	0.862	0.68 ± 0.10	3.30	1.64 ± 0.25
^{11}C	2.89	4.70 ± 0.71	4.47	7.05 ± 1.06	6.26	9.64 ± 1.45	23.5	22.0 ± 3.3
^{13}N	0.332	0.23 ± 0.05	0.337	0.28 ± 0.06	0.321	0.44 ± 0.09	0.425	0.63 ± 0.13
^{15}O	0.87	1.53 ± 0.23	1.39	2.35 ± 0.35	2.06	3.19 ± 0.48	5.10	5.14 ± 0.77

^3He in water and PMMA, are underpredicted at all ^3He energies. This means that there is a room for improvement of the GEANT4 nuclear reaction models with respect to ^3He -induced reactions.

5. Calculations of β^+ -activity distributions in tissues

As demonstrated above, the total yields and spatial distributions of β^+ -activity produced by therapeutic beams depend essentially on the elemental compositions of target materials. Therefore, for studying the feasibility of the PET monitoring method in real tissues irradiated with ^3He we have performed calculations for two homogeneous phantoms with elemental composition similar to muscle ($9 \times 9 \times 30 \text{ cm}^3$, $\rho = 1.061 \text{ g cm}^{-3}$) and compact bone ($9 \times 9 \times 15 \text{ cm}^3$, $\rho = 1.850 \text{ g cm}^{-3}$). The elemental composition was taken in the following mass fractions: H - 10.2 %, C - 14.3%, N - 3.4 %, O - 71%, Na - 0.1 %, P - 0.2%, S - 0.3 %, Cl - 0.1 %, K - 0.4% for muscle tissue, and H - 6.4 %, C - 27.8%, N - 2.7 %, O - 41%, Mg - 0.2 %, P - 7%, S - 0.2 %, Ca - 14.7 % for compact bone tissue. The beam parameters in calculations of ^3He irradiation of muscle (bone) were taken the same as for ^3He beam in water (graphite), as listed in Table 1. The calculated depth distributions of β^+ -activity in tissues irradiated by 207.92 A MeV ^3He are shown in Figs. 7 and 8.

Due to the presence of Na, P, S, Cl, Ca, K and Mg in muscle and bone tissues, ^{19}Ne ($T_{1/2} = 17.22 \text{ s}$), ^{21}Na ($T_{1/2} = 22.49 \text{ s}$), and ^{30}P ($T_{1/2} = 2.498 \text{ min}$) can also be produced in fragmentation reactions in addition to the isotopes analysed in the previous sections. However, only negligible yields of ^{19}Ne and ^{21}Na are predicted by the MCHIT model and they can be safely neglected. The β^+ -activity distributions in muscle are similar to those in water (c.f. Fig. 2). In bone tissue, however, ^{30}P is additionally produced by the ^{31}P target fragmentation. In fact, both ^{30}P and ^{15}O noticeably contribute to the dN_{β^+}/dz after the distal edge of the Bragg peak, as shown in Fig. 8. This is similar to ^{11}C distribution in graphite and PMMA irradiated by ^3He (see Figs. 1 and 3 where also a tail of the β^+ -activity is present beyond the Bragg peak).

Only ^{11}C and ^{18}F survive in muscle and bone tissues at later time after irradiation. The presence of ^{18}F opens a new way to monitor the ^3He range in tissues, as the ^{18}F peak (see the bottom panels of Figs. 7 and 8) clearly mark the position of the Bragg peak.

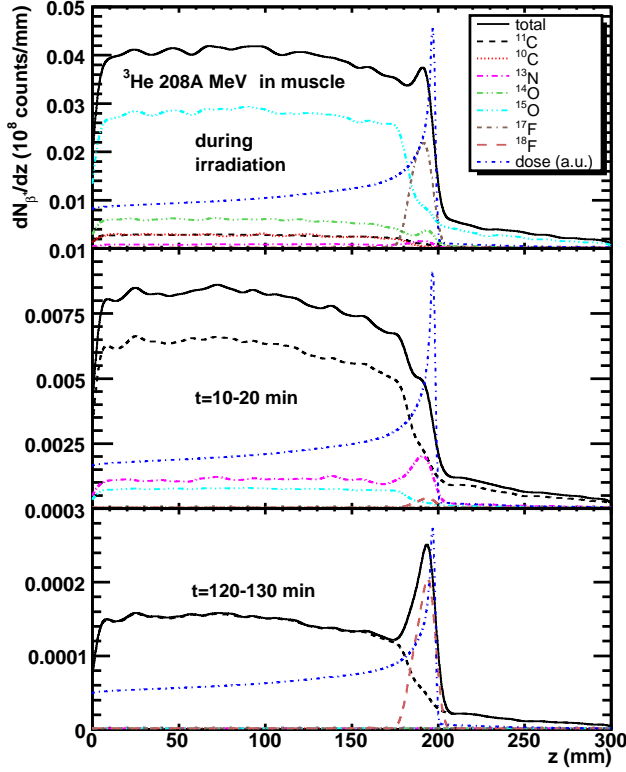


Figure 7. Depth distribution of β^+ -activity induced by 207.92 A MeV ^3He beam in muscle tissue. The distributions of β^+ -decays counted during irradiation, from 10 to 20 min and from 120 to 130 min after it are shown by solid lines in top, middle and bottom panels, respectively. Contributions of specific isotopes and depth-dose distribution are also shown, as explained on the legend.

6. PET monitoring with low energy proton, ^3He and ^{12}C beams

The nuclear pick-up reactions leading to the production of ^{14}O , ^{17}F and ^{18}F nuclei have the maximal cross sections at low energies. In this energy regime the velocities of projectile nuclei are comparable to the velocities of intranuclear nucleons due to Fermi motion. This gives optimum conditions for transferring nucleons from one collision partner to another during their collision and enhances the production of ^{14}O , ^{17}F and ^{18}F .

It is instructive to consider the distributions of β^+ -activity in muscle produced by various low-energy beams during irradiation, as shown in Fig. 9. In these calculations the time structure of all three beams was assumed the same as for graphite irradiation by ^3He , see Table. 1. It is expected that nuclear transfer reactions are more important at low energies, while nuclear fragmentation reactions contribute less because they have certain energy thresholds.

As one can see in Fig. 9, the distribution of positron emitting nuclei produced by low-energy 87 MeV proton beam is almost uniform and poorly correlated with the position of the Bragg peak. In fact, the Bragg peak in the depth-dose distribution is located at the region with a negligible β^+ -activity. A similar distribution is predicted

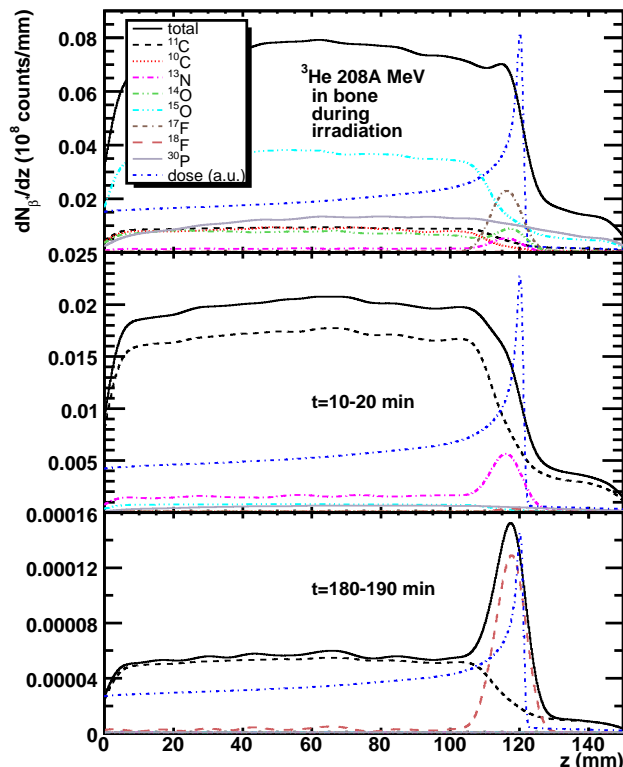


Figure 8. Same as Fig. 7, but for 207.92 A MeV ^3He beam in compact bone tissue and for β^+ -decays counted from 180 to 190 min after irradiation (bottom panel).

for ^{15}O produced by 102 A MeV ^3He . However, ^{17}F nuclei are additionally produced by ^3He in nuclear charge pick-up reactions close to the Bragg peak. This makes the total distribution of β^+ -activity for ^3He more suitable for the determination of the ^3He range in tissues by the PET method, as the distal end of the β^+ -activity distribution marks clearly the position of the Bragg peak. It is advisable to perform the PET measurements with low-energy ^3He beams to quantify the contribution of charge pick-up reactions. The β^+ -activity distribution produced by 162 A MeV ^{12}C is also suitable for PET monitoring due to the presence of broad peaks associated with ^{10}C and ^{11}C nuclei.

7. Reliability of calculational results

We discuss the discrepancies between the MCHIT results and the experimental data by Fiedler *et al* 2006. The calculations agree with the data on the total yields of ^{10}C , ^{11}C , ^{13}N and ^{15}O in graphite, water and PMMA at $\sim 30 - 50\%$ accuracy level, see Tables 2-4. However, the agreement with the activity distribution measured 10-20 min after irradiation of water by 207.92 A MeV ^3He is poor, see the middle panel of Fig. 3. We identify this discrepancy with the poor description of $^{16}\text{O}(^3\text{He},4\text{p}4\text{n})^{11}\text{C}$ reaction, and we conclude that it has to be improved in GEANT4. In this reaction

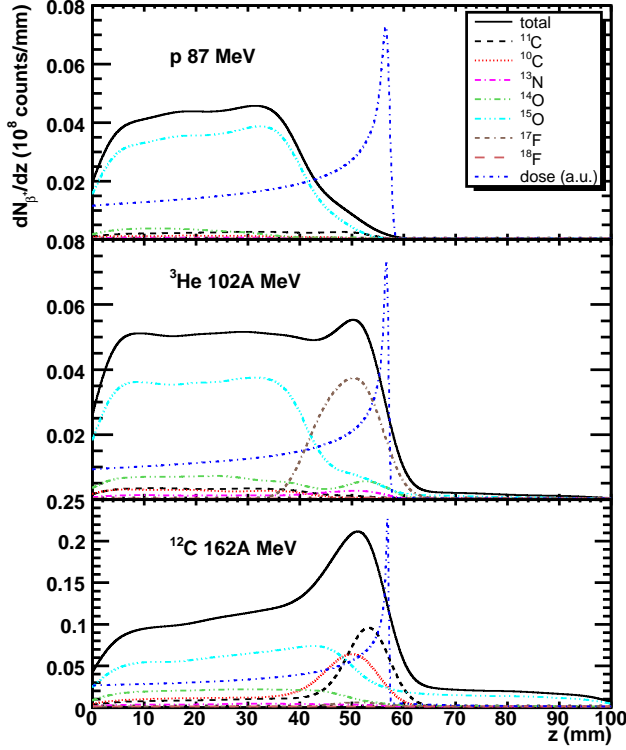


Figure 9. Depth distribution of β^+ -activity during irradiation by 87 MeV protons (top panel), 102 A MeV ^3He (middle panel) and 162 A MeV ^{12}C beam in muscle tissue.

a compound nucleus ^{19}Ne can be created leading to a larger longitudinal momentum transfer as compared with the direct mechanism. Therefore, the ^{11}C nuclei produced in decays of ^{19}Ne will have on average a larger longitudinal momentum and will stop closer to the Bragg peak. Therefore, the agreement in shapes of the calculated and measured distributions of ^{11}C nuclei can be possibly improved by taking into account the formation of ^{19}Ne .

The model was also confronted with the measured activity distributions from 337.5 A MeV ^{12}C in graphite, water and PMMA. The largest discrepancy between calculations and data obtained 10-20 min after irradiation was found for the graphite phantom, see the bottom panel of Fig. 4. To identify the origin of this discrepancy the cross section $\sigma(^{11}\text{C})$ of the $^{12}\text{C}(^{12}\text{C},n)^{11}\text{C}$ reaction was calculated with the GEANT4 toolkit. This was done following the expression:

$$\sigma(^{11}\text{C}) = \frac{dN_{^{11}\text{C}}}{dz} \bigg|_{z=0} n^{-1}, \quad (11)$$

where $dN_{^{11}\text{C}}/dz|_{z=0}$ is the number of ^{11}C nuclei per incident ^{12}C ion per unit length at the entrance point $z = 0$ to the graphite. In fact, we have averaged $dN_{^{11}\text{C}}/dz$ over the region $0 < z < 1$ mm. The ^{12}C concentration in graphite is $n = 9 \cdot 10^{22} \text{ cm}^{-3}$. The obtained results are compared with the data by Yashima *et al* 2003, 2004 in Table 5. One can see that the MCHIT model overpredicts the cross section $\sigma(^{11}\text{C})$

by 30-60%. The ratio $\sigma_{^{11}\text{C}}^{\text{GEANT4}}/\sigma_{^{11}\text{C}}^{\text{exp}}$ seems to grow at lower beam energies. This explains the shift of the peak of the calculated activity distribution to larger z with respect to the data.

Table 5. Cross section of the reaction $^{12}\text{C}(^{12}\text{C},\text{X})^{11}\text{C}$ calculated using GEANT4 in comparison to the data from Yashima *et al* 2003, 2004 . The error bars on theoretical results are pure statistical.

E/A, MeV	$\sigma_{^{11}\text{C}}^{\text{GEANT4}}$, mb	$\sigma_{^{11}\text{C}}^{\text{exp}}$, mb
100	144 \pm 14	88.3 \pm 3.2
230	106 \pm 17	79.0 \pm 7.9
400	100 \pm 10	68.6 \pm 2.5

The production of ^{18}F by 36-40 MeV ^3He ions in water was studied by Fitschen *et al* 1977 and by Knust and Machulla 1983 . They reported 20 mCi/ μA and 19 mCi/ μA activity of ^{18}F after 3 and 2.5 hours of irradiation with ^3He beam, respectively. The activity calculated by the MCHIT model for similar irradiation conditions amounts to 18.7 mCi/ μA , which is in very good agreement with the experimental yields. This analysis shows that the low-energy nuclear data play an important role in designing reliable models for heavy-ion cancer therapy.

8. Summary and conclusions

We have considered nuclear reactions induced by ^3He and ^{12}C beams in tissue-like materials from the view point of their suitability for PET monitoring. As found, in addition to nuclear fragmentation reactions of projectile and target nuclei, leading to creation of $^{10,11}\text{C}$ and $^{14,15}\text{O}$, the contributions from several nuclear pick-up reactions, $^{12}\text{C}(^3\text{He},\text{X})^{13}\text{N}$, $^{12}\text{C}(^3\text{He},\text{n})^{14}\text{O}$, $^{16}\text{O}(^3\text{He},\text{X})^{17}\text{F}$ and $^{16}\text{O}(^3\text{He},\text{p})^{18}\text{F}$ must be taken into account. The pick-up of nucleons is quite efficient at low collision energies when the relative velocities of nuclei are comparable to the characteristic velocities of intranuclear nucleons due to their Fermi motion. On the other hand, it is known that this is the region of ion-beam energies with the maximum of relative biological effectiveness (RBE).

As pointed out a long time ago by Osgood *et al* 1964, Cirilov *et al* 1966 and Hahn and Ricci 1966, there exist different mechanisms of pick-up reactions. Indeed, the proton stripping reaction $^{12}\text{C}(^3\text{He},\text{d})^{13}\text{N}$ is a direct reaction, while the $^{12}\text{C}(^3\text{He},\text{n})^{14}\text{O}$ process goes through the formation of ^{15}O compound nucleus. In both cases, the reaction cross section increases at low projectile energies. As follows from our calculations, ^{13}N and ^{14}O are concentrated near the Bragg peak of ^3He in graphite and PMMA (Figs. 1 and 3), while the distributions of ^{10}C , ^{11}C and ^{15}O are flat because such nuclides are resulting from target fragmentation reactions.

The process $^{16}\text{O}(^3\text{He},\text{p})^{18}\text{F}$ is of particular interest since ^{18}F is a long living isotope ($T_{1/2} = 109.77$ min), making it suitable for off-line monitoring of β^+ -activity. According to Hahn and Ricci 1966, the cross section of this reaction has a maximum 436 ± 44 mb at $E_{\text{lab}} = 6.3$ MeV and drops at higher beam energies. As demonstrated above, 2-3 hours after irradiation by ^3He a peak in the β^+ -activity distribution due to ^{18}F is developed in water and PMMA. The position of this peak well matches the position of the Bragg peak. Counting statistics in the experiment by Fiedler *et al* 2006

should, in principle, allow to identify this peak. Since the measured biological wash-out time is about of 91-124 min in muscle (Tomitani *et al* 2003), i.e. comparable to physical half-life of ^{18}F , the biological wash-out should not drastically decrease PET signal even for water-dominated tissues. In bone tissue PET signal is expected to be robust and survive 2-3 hours after irradiation. Alternatively, the biological wash-out of β^+ -activity at later times (≥ 1 hour) may be studied with ^{18}F .

Acknowledgments

This work was supported by Siemens Medical Solutions. We are grateful to Prof. Hermann Requardt for stimulating discussions. The discussions with Dr. Thomas Haberer and Dr. Dieter Schardt are gratefully acknowledged. We are indebted to Prof. Wolfgang Enghardt and Dr. Fine Fiedler for discussions and for providing us with the tables of their experimental data, and their compilation of experimental data on ^3He -induced nuclear reactions.

References

- Agostinelli S *et al* (GEANT4 Collaboration) 2003 GEANT4: A simulation toolkit *Nucl. Instrum. Methods A* **506** 250-303
- Allison J *et al* (GEANT4 Collaboration) 2006 GEANT4 developments and applications *IEEE Trans. Nucl. Sci.* **53** 270-8
- Amaldi U and Kraft G 2005 Radiotherapy with beams of carbon ions *Rep. Prog. Phys.* **68** 1861-82
- Amaldi U 2004 CNAO—The Italian Centre for Light-Ion Therapy *Radiother. Oncol.* **73** S191-201
- Bajard M, De Conto J M and Remillieux J 2004 Status of the "ETOILE" project for a French hadrontherapy centre *Radiother. Oncol.* **73** S211-5
- Bennett G W, Goldberg A C, Levine G S, Guthy J, Balsamo J and Archambeau J O 1975 Beam localization via O-15 activation in proton-radiation therapy *Nucl. Instr. Methods* **125** 333-8
- Bennett G W, Archambeau J O, Archambeau B E, Meltzer J I and Wingate C L 1978 Visualization and transport of positron emission from proton activation in vivo *Science* **200** 1151-3
- Bondorf J P, Botvina A S, Iljinov A S, Mishustin I N and Sneppen K 1995 Statistical multifragmentation of nuclei *Phys. Rept.* **257** 133-221
- Castro J R, Petti P L, Blakely E A and Daftari I K 2004 Particle radiation therapy *Textbook of Radiation Oncology* (Saunders, Elsevier Inc.) ed Leibel S A and Phillips T L pp 1547-68
- Cirilov S D, Newton J O and Schapira J P 1966 Total cross sections for the reaction $^{12}\text{C}(^3\text{He},\alpha)^{11}\text{C}$ and $^{12}\text{C}(^3\text{He},n)^{14}\text{O}$ *Nucl. Phys.* **77** 472-6.
- Enghardt W, Crespo P, Fiedler F, Hinz R, Parodi K, Pawelke J, and Pönisch F 2004 Charged hadron tumour therapy monitoring by means of PET *Nucl. Instrum. Methods A* **525** 284-8
- Enghardt W, Fromm W D, Geissel H, Keller H, Kraft G, Magel A, Manfrass P, Munzenberg G, Nickel F, Pawelke J, Schardt D, Scheidenberger C and Sobiella M 1992 The spatial-distribution of positron-emitting nuclei generated by relativistic light-ion beams in organic-matter *Phys. Med. Biol.* **37** 2127-31
- Fiedler F, Crespo P, Parodi K, Sellesk M and Enghardt W 2006 The feasibility of in-beam PET for therapeutic beams of ^3He *IEEE Trans. Nucl. Sci.* **53** 2252-9
- Fitschen J, Beckmann R, Holm U and Neuert H 1977 Yield and production of ^{18}F by ^3He irradiation of water *Int. J. Appl. Radiat. Isot.* **28** 781-884
- Folger G, Ivanchenko V N and Wellisch J P 2004 The Binary Cascade - nucleon-nuclear reactions *Eur. Phys. J. A* **21** 407-17
- Furusawa Y, Fukutsu K, Aoki M, Itsukaichi H, Eguchi-Kasai K, Ohara H, Yatagai E, Kanai T and Ando K 2000 Inactivation of aerobic and hypoxic cells from three different cell lines by accelerated ^3He , ^{12}C and ^{20}Ne -ion beams *Radiat. Res.* **154** 485-96
- GEANT4-Documents 2006 <http://geant4.web.cern.ch/geant4/G4UsersDocuments/Overview/html/>
- GEANT4-Webpage 2006 <http://geant4.web.cern.ch/geant4/>
- Griesmayer E and Auberger T 2004 The status of MedAustron *Radiother. Oncol.* **73** S202-5
- Haberer T, Debus J, Eickhoff H, Jakel O, Schulz-Ertner D and Weber U 2004 The Heidelberg ion therapy center *Radiother. Oncol.* **73** S186-90

- Hahn R L and Ricci E 1966 Interactions of ^3He Particles with ^9Be , ^{12}C , ^{16}O and ^{19}F *Phys. Rev.* **146** 650-9.
- Heeg P, Eickhoff H and Haberer T 2004 Conception of heavy ion beam therapy at Heidelberg University (HICAT) *Z. Med. Phys.* **14** 17-24
- Hishikawa Y, Oda Y, Mayahara H, Kawaguchi A, Kagawa K, Murakami M and Abe M 2004 Status of the clinical work at Hyogo *Radiother. Oncol.* **73** S38-40
- Hishikawa Y, Kagawa K, Murakami M, Sakai H, Akagi T and Abe M 2002 Usefulness of positron-emission tomographic images after proton therapy *Int. J. Radiat. Oncol. Biol. Phys.* **53** 1388-91
- Kempe J, Gudowska I and Brahme A 2007 Depth absorbed dose and LET distributions of therapeutic ^1H , ^4He , ^7Li and ^{12}C beams *Med. Phys.* **34** 183-92
- Knust E J and Machulla H-J 1983 High yield production of ^{18}F in water target via the $^{16}\text{O}(^3\text{He},\text{p})^{18}\text{F}$ reaction *Int. J. Appl. Radiat. Isot.* **34** 1627-8
- Levin C S and Hoffman E J 1999 Calculation of positron range and its effect on the fundamental limit of positron emission tomography system spatial resolution *Phys. Med. Biol.* **44** 781-99
- Nishio T, Sato T, Kitamura H, Murakami K and Ogino T 2005 Distributions of β^+ decayed nuclei generated in the CH_2 and H_2O targets by the target nuclear fragment reaction using therapeutic MONO and SOBP proton beam *Med. Phys.* **32** 1070-82
- Oelfke U, Lam G K and Atkins M S 1996 Proton dose monitoring with PET: quantitative studies in Lucite *Phys. Med. Biol.* **41** 177-96
- Osgood D R, Patterson J R and Titterton E W 1964 The excitation function for reaction $\text{C}^{12}(\text{He}^3, \text{n}_0)\text{O}^{14}$ between threshold and 11.45 MeV *Nucl. Phys.* **60** 503-8
- Parodi K and Enghardt W 2000 Potential application of PET in quality assurance of proton therapy *Phys. Med. Biol.* **45** N151-6
- Parodi K, Enghardt W and Haberer T 2002 In-beam PET measurements of β^+ radioactivity induced by proton beams *Phys. Med. Biol.* **47** 21-36
- Parodi K 2004 On the feasibility of dose quantification with in-beam PET data in radiotherapy with ^{12}C and proton beams 2004, Ph.D. Dissertation, Technische Universität Dresden.
- Parodi K, Ferrari A, Sommerer F and Paganetti H 2007a Clinical CT-based calculations of dose and positron emitter distributions in proton therapy using the FLUKA Monte Carlo code *Phys. Med. Biol.* **52** 3369-87
- Parodi K, Paganetti H, Shih H A, Michaud S, Loeffler J S, DeLaney T F, Liebsch N J, Munzenrider J E, Fischman A J, Knopf A and Bortfeld T 2007b Patient study of in vivo verification of beam delivery and range, using positron emission tomography and computed tomography imaging after proton therapy *Int. J. Radiat. Oncol. Biol. Phys.* **68** 920-34
- Pawelke J, Byars L, Enghardt W, Fromm W D, Geissel H, Hasch B G, Lauckner K, Manfrass P, Schardt D and Sobiella M 1996 The investigation of different cameras for in-beam PET imaging *Phys. Med. Biol.* **41** 279-96
- Pawelke J, Enghardt W, Haberer T, Hasch B G, Hinz R, Kramer M, Lauckner K and Sobiella M 1997 In-beam PET imaging for the control of heavy-ion tumour therapy *IEEE Trans. Nucl. Sci.* **44** 1492-8
- Pönisch F, Parodi K, Hasch B G and Enghardt W 2004 The modelling of positron emitter production and PET imaging during carbon ion therapy *Phys. Med. Biol.* **49** 5217-32
- Pshenichnov I, Mishustin I and Greiner W 2005 Neutrons from fragmentation of light nuclei in tissue-like media: a study with the GEANT4 toolkit *Phys. Med. Biol.* **50** 5493-507
- Pshenichnov I, Mishustin I and Greiner W 2006 Distributions of positron-emitting nuclei in proton and carbon-ion therapy studied with GEANT4 *Phys. Med. Biol.* **51** 6099-112
- Schulz-Ertner D, Nikoghosyan A, Thilmann C, Haberer T, Jakel O, Karger C, Kraft G, Wannenmacher M and Debus J 2004 Results of carbon ion radiotherapy in 152 patients *Int. J. Radiat. Oncol. Biol. Phys.* **58** 631-40
- Shen W, Wang B, Feng J, Zhan W, Zhu Y and Feng E Total reaction cross-section for heavy-ion collisions and its relation to the neutron excess degree of freedom *Nucl. Phys. A* **491** 130-46
- Tomitani T, Pawelke J, Kanazawa M, Yoshikawa K, Yoshida K, Sato M, Takami A, Koga M, Futami Y, Kitagawa A, Urakabe E, Suda M, Mizuno H, Kanai T, Matsuura H, Shinoda I and Takizawa S 2003 Washout studies of ^{11}C in rabbit thigh muscle implanted by secondary beams of HIMAC *Phys. Med. Biol.* **48** 875-89
- Tripathi R K, Cucinotta F A and Wilson J W 1999 Universal parameterization of absorption cross sections, NASA Technical Paper 3621
- Tsujii H, Mizoe J E, Kamada T, Baba M, Kato S, Kato H, Tsuji H, Yamada S, Yasuda S, Ohno T, Yanagi T, Hasegawa A, Sugawara T, Ezawa H, Kandatsu S, Yoshikawa K, Kishimoto R and Miyamoto T 2004 Overview of clinical experiences on carbon ion radiotherapy at NIRS. *Radiother. Oncol.* **73** S41-9

- Weisskopf V E and Ewing D H 1940 On the yield of nuclear reactions with heavy elements *Phys. Rev.* **57** 472-85
- Wellisch H P and Axen D 1996 Total reaction cross section calculations in proton-nucleus scattering *Phys. Rev. C* **54** 1329-32
- Yashima H, Uwamino Y, Iwase H, Sugita H, Nakamura T, Ito S and Fukumura A 2003 Measurement and calculation of radioactivities of spallation products by high-energy heavy ions *Radiochim. Acta* **91** 689-96
- Yashima H, Uwamino Y, Iwase H, Sugita H, Nakamura T, Ito S, Fukumura A 2004 Cross sections for the production of residual nuclides by high-energy heavy ions *Nucl. Instr. Methods B* **226** 243-63